

# Apparent scale correlations in a random multifractal process

Jochen Cleve<sup>1</sup>, Jürgen Schmiegel<sup>2</sup>, and Martin Greiner<sup>1</sup>

<sup>1</sup> Corporate Technology, Information&Communications, Siemens AG, D-81730 München, Germany

<sup>2</sup> Thiele Centre for Applied Mathematics in Natural Science, Aarhus University, DK-8000 Aarhus, Denmark

April 10, 2008

**Abstract.** We discuss various properties of a homogeneous random multifractal process, which are related to the issue of scale correlations. By design, the process has no built-in scale correlations. However, when it comes to observables like breakdown coefficients, which are based on a coarse-graining of the multifractal field, scale correlations do appear. In the log-normal limit of the model process, the conditional distributions and moments of breakdown coefficients reproduce the observations made in fully developed small-scale turbulence. These findings help to understand several puzzling empirical details, which have been extracted from turbulent data already some time ago.

**PACS.** 47.27.eb Statistical theories and models – 47.27.Gs Isotropic turbulence; homogeneous turbulence – 47.53.+n Fractals in fluid dynamics – 02.50.Ey Stochastic processes – 02.50.Ga Markov processes

## 1 Introduction

In the context of fully developed turbulence deviations from the pioneering K41 scaling prediction [1] are well described with the multifractal formalism and have led to the empirical modeling of the turbulent energy cascade with random multiplicative cascade processes [2–6]. By design, the random multiplicative transfer of energy flux from the integral down to the dissipation scale comes with no scale correlations. However, this model property has not been confirmed in a first data inspection based on breakdown coefficients of the energy dissipation [7, 8]. Another, Markovian-based approach [9, 10] supports this finding, that the turbulent energy cascade appears to come with inherent scale correlations. It is exactly this conflict which motivates us to look closer into the nature of scale correlations of random multifractal processes in general and of the turbulent energy cascade in particular.

Previous work in this direction has focused on binary discrete random multiplicative cascade processes. Their non-conservative variants were able to explain the observed scale-independent unconditional distributions of breakdown coefficients [7, 8] as fixed points resulting from small-scale resummation [11, 12], which are also different from the employed cascade generator. Furthermore, by adopting an experimentalist’s view, who is not aware of the underlying tree-like hierarchy of the cascade process and who then homogeneously samples observables, the correlations observed in the conditional distributions of breakdown coefficients [7, 8] had been reproduced, especially when the cascade generator is chosen to be positively skewed [13]. With the same overall approach, also the observed scale-dependence of Kramers-Moyal coeffi-

cients, representing the Markovian description of the turbulent energy cascade [9, 10], had been reproduced qualitatively [14].

So far the qualitative success to explain the observed scale correlations out of non-scale-correlated models is tied to binary discrete random multiplicative cascade processes. Of course, this is subject to some criticism. First of all, the turbulent energy cascade is neither binary nor discrete. Second, although plausible from a physics perspective, the employed small-scale resummation as well as the experimentalist’s homogeneous sampling appear to be operationally rather ad hoc. In this respect it would be nice to consider more general and more elegant stochastic multifractal processes, which are not in need of ad hoc operations, and which hopefully not only confirm the previous findings, but also put them on more firm ground and allow to resolve some more of the empirically observed and quantified puzzling details.

This is exactly what we are going to demonstrate. Various elegant stochastic multifractal processes have been proposed in Refs. [15–20]. They are closely related to each other, but have originated from different backgrounds like turbulence, finance and Internet data-traffic engineering. They are all continuous and homogeneous. The random multifractal log-stable process of Ref. [20] will be briefly presented in Sect. 2. It does not have built-in scale correlations, but, as we will see in Sects. 3 and 4, when it comes to the analysis of breakdown coefficients and Kramers-Moyal coefficients the scale correlations do appear again. The precision reached within these simulations allows for several further quantitative statements: (i) the obtained distributions of breakdown coefficients allow no room for log-stable statistics of the energy dissipation, except when

close to the log-normal limit; (ii) extracted moments of breakdown coefficients reproduce the puzzling systematics on apparent scaling exponents, observed and discussed in Refs. [8,21]; (iii) the two differing outcomes of the extracted Kramers-Moyal coefficients [9,10] are reproduced and trace back to different operational definitions; (iv) the intermittency exponent can be extracted with reasonable precision from the first Kramers-Moyal coefficient. A conclusion and outlook will be given in Sect. 5.

## 2 Modeling of a continuous and homogeneous random multifractal process

In Ref. [20], see Refs. [15–19] for related approaches, a positive-valued multifractal field  $\varepsilon(x, t)$  on continuous 1+1 space-time has been designed as the stochastic integral

$$\varepsilon(x, t) = \exp \left\{ \int_{t-T}^t dt' \int_{x-g(t-t')}^{x+g(t-t')} dx' \gamma(x', t') \right\}. \quad (1)$$

$\gamma(x, t) \sim S_\alpha((dxdt)^\alpha)^{-1} \sigma, -1, \sigma^\alpha / \cos(\pi\alpha/2)$  is assumed to be a Lévy-stable white-noise field [22] with property  $\langle \exp\{\gamma\} \rangle = 1$ . The causality cone

$$g(t-t') = \frac{L}{2} \min \left\{ \left( 1 + \frac{(L-\eta)(T-\Delta T-(t-t'))}{\eta(T-\Delta T)} \right)^{-1}, 1 \right\} \quad (2)$$

has the properties  $g(T-\Delta T) = g(T) = L/2$  and  $g(0) = \eta/2$ , with  $L \gg \eta$  representing the integral and dissipation length, and  $T \gg \Delta T$  the integral time and a convenient cutoff; consult Fig. 1 and see Ref. [20] for more details.

The explicit shape (2) allows to express the field (1) at spatio-temporal position  $x, t$  as a product

$$\varepsilon(x, t) \sim \prod_{j=1}^J q_j \quad (3)$$

of independently and identically distributed (iid) random weights

$$q_j = q(x, t; l_j) = \exp \left\{ \int_{t-t_{j-1}}^{t-t_j} dt' \int_{x-g(t-t')}^{x+g(t-t')} dx' \gamma(x', t') \right\}. \quad (4)$$

The latter are associated to the hierarchy of scales  $l_j = L/\lambda^j = 2g(T-t_j)$  confined by  $\eta = l_J$  and  $L = l_0$ . In Fig. 1 they are illustrated as hatched stripes. Since these stripes are non-overlapping and have identical spatio-temporal size, and since  $\gamma(x, t)$  is a homogeneous Lévy-stable white-noise field, the multiplicative random weights  $q_j$  are iid and are not correlated to each other. This reflects the spirit of random multiplicative cascade processes and demonstrates that no scale correlations are build into the ansatz (1).

Furthermore, with the setting  $\Delta T/T = \eta/L$  Eqs. (1) and (2) directly lead to perfect scaling of the equal-time two-point correlation densities

$$\frac{\langle \varepsilon^{n_1}(x_1, t) \varepsilon^{n_2}(x_2, t) \rangle}{\langle \varepsilon^{n_1}(x_1, t) \rangle \langle \varepsilon^{n_2}(x_2, t) \rangle} = \left( \frac{L}{|x_2 - x_1|} \right)^{\tau_{n_1+n_2} - \tau_{n_1} - \tau_{n_2}} \quad (5)$$

for two-point distances  $\eta \leq |x_2 - x_1| \leq L$ . For larger distances the correlations are equal to one. The multifractal scaling exponents are given by  $\tau_n = \tau_2(n^\alpha - n)/(2^\alpha - 2)$  with  $\tau_2 = (\sigma^\alpha / \cos \frac{\pi\alpha}{2})(2 - 2^\alpha)\eta T$ . See again Ref. [20] for more details.

Besides  $L, T$  and  $\eta$ , the only other independent parameters of the stochastic process (1) are the Lévy-stable index  $0 \leq \alpha \leq 2$  and  $\sigma$ . In Sect. 3 we will discuss various combinations of the latter, which turn out to be relevant for the breakdown coefficients observed in fully developed turbulence. – In [20] the parameters  $\alpha$  and  $\sigma$  have been fixed by the observed scaling exponents  $\tau_2$  and  $\tau_3$  extracted from the lowest-order two-point correlation densities. With no room left for further adjustments the predicted three-point correlation densities have been shown to be in excellent agreement with their counterparts from turbulent energy-dissipation data.

All further results to be presented in the following have been obtained from simulations based on a straightforward implementation of Eq. (1). Only equal-time traces  $\varepsilon(x) = \varepsilon(x, t)|_{t=\text{const}}$  have been produced. The numerical resolutions have been set to  $\Delta x = \Delta t = \eta/6$  for the noise field  $\gamma(x, t)$  and  $\Delta x = \eta$  for the equal-time trace  $\varepsilon(x)$ , respectively. Fig. 2 shows a fraction of a simulated equal-time trace; the intermittent behavior clearly resembles the fluctuations observed for the energy dissipation of real fully developed turbulent flows. Observables like two-point correlation densities, breakdown coefficients and Kramers-Moyal coefficients have been sampled from one simulated equal-time trace of length  $L_{\text{trace}} = 10^7 \eta = 2 \times 10^4 L$ . Of course, different time traces have been produced for different parameter values  $\alpha$  and  $\sigma$ . The other remaining model parameters  $L/\eta = 500$  and  $T = L$  have been kept fixed and represent a typical inertial-range length of fully developed turbulent flows relevant to the observations made for the breakdown and Kramers-Moyal coefficients [7–10, 23, 24]. The employed numerical resolutions  $\Delta x, \Delta t$  and the sampling cutoff  $L_{\text{trace}}$  have produced sufficient convergence for all considered observables. For example, Fig. 3 shows the such sampled lowest-order two-point correlation density. It reproduces (5) with high quality. A rougher resolution for the noise field  $\gamma(x, t)$  results in a noticeable deviation.

## 3 Apparent scale-correlations I: breakdown coefficients

The breakdown coefficients

$$b(x; l, \lambda, \Delta) = \frac{\varepsilon_{l/\lambda}(x + l\Delta(\lambda - 1)/\lambda)}{\varepsilon_l(x)} \quad (6)$$

are defined as the ratio of coarse-grained field amplitudes

$$\varepsilon_l(x) = \frac{1}{l} \int_{x-l/2}^{x+l/2} \varepsilon(x') dx' \quad (7)$$

at scales  $l/\lambda$  and  $l$ , separated by the scale parameter  $\lambda > 1$ . The parameter  $\Delta$  describes the relative position between parent and offspring interval.  $\Delta = 0$  corresponds to the centered case and  $\Delta = \pm 1/2$  to right- and left-alignment, respectively; see the insets of Figs. 4 and 5 for an illustration. For turbulent cascades at high Reynolds numbers, scale-independence of unconditional distributions of breakdown coefficients has been observed in the upper part of the inertial range [7, 8, 23, 24] and has been thought to describe the cascade generator [24–27], thus allowing for an alternative approach to analyze multifractality. However, by construction the breakdown coefficients (6) are different from the log-stable random multiplicative weights  $q(l)$  of (4). This is further emphasized in Fig. 4a, which illustrates the unconditional distribution of left/right-sided  $\lambda = 2$  breakdown coefficients sampled from simulated model traces. Within the upper cascade regime  $20\eta \leq l \leq L$  these distributions are found to be independent of the scale  $l$ ; for smaller and larger scales they are more narrow. The shown distributions are not of log-stable type; see Fig. 4b and also Fig. 5b. They can be nicely parametrized with a symmetric Beta-distribution  $p(b) \sim b^{\beta-1}(2-b)^{\beta-1}$ . For the log-normal setting  $\alpha = 2.0$  and  $\tau(2) = 0.24$  of the model parameters the found distribution nicely matches the distribution reported in the analysis of a high-Reynolds number atmospheric boundary layer [7].

Upon switching from unconditional to conditional distributions scale correlations do appear. When conditioned onto a large (small) parent breakdown coefficient, the distribution with  $\lambda = 2$ ,  $\Delta = \pm 1/2$  of Fig. 5a(top left) results to be broader (more narrow) than its unconditional counterpart. This outcome is in full agreement with the experimental findings reported in [7]. Fig. 5a(top right) shows the related centered distributions. In its unconditional form it is again well described with a symmetric Beta distribution, but now with increased exponent  $\beta = 4.9$ . For a large parent breakdown coefficient the distribution is broadened and shifted to the right, whereas it is narrowed and shifted to the left once the parent is small. These findings are in perfect agreement with the experimental observations presented in [8]. This demonstrates that the scale correlations reported in [7, 8] can be fully reproduced by the stochastic process (1), which by construction has no built-in scale correlations. – But where do the scale correlations come from? They trace back to the coarse-graining (7) of the non-conservative multifractal field. This correlates the breakdown coefficient to its parent.

So far only the log-normal limit  $\alpha = 2$  of (1) has been discussed. With the same choice  $\tau_2 = 0.24$  for the intermittency exponent, the second and third rows of Fig. 5 illustrate the distributions of  $\lambda = 2$  breakdown coefficients for  $\alpha = 1.7$  and  $1.4$ , respectively. With decreasing  $\alpha$  the differences between conditional and unconditional  $\Delta = \pm 1/2$  distributions also decrease, leading to a disap-

pearance of the scale correlations at  $\alpha \approx 1.4$ . Note also another detail for  $\alpha < 2$ : all distributions increase again as the breakdown coefficient approaches zero (two) from above (below). This effect becomes stronger the smaller  $\alpha$  is chosen and is a fingerprint of the excess probability  $p(q = 0^+) > 0$  occurring for log-stable distributions; see also Fig. 5b. Also the distributions of centered breakdown coefficients reveal an interesting behavior with  $\alpha$ . Whereas for  $\alpha = 2$  the left-shifted conditional distribution has a larger maximum than the right-shifted one, the two maxima become about equal for  $\alpha = 1.7$  and reverse their order for  $\alpha = 1.4$ . In comparison with the experimental observations [7, 8] these findings suggest that the stability index  $\alpha$  should be two, or at least very close to two. Except for the log-normal limit, this leaves no room for the log-stable modeling of the turbulent energy cascade [28, 29]. Put into a more general context, scale correlations observed in conditional distributions of breakdown coefficients allow for a sensitive parameter estimation of universal multifractals [30]. – For the remainder of this Article we adopt the log-normal limit  $\alpha = 2$ , where the Lévy-stable white-noise field of (1) corresponds to a non-centered Gaussian white-noise field.

Up to now we have only investigated breakdown coefficients with a scale ratio of  $\lambda = 2$ , but there is no reason to restrict the analysis to this scale ratio. Model simulations reveal that as for  $\lambda = 2$ , the distributions of breakdown coefficients for arbitrary  $1 < \lambda < 2$  turn out to be scale-independent within the upper part  $20\eta \leq l \leq L$  of the cascade range. They can be well described with asymmetric Beta distributions  $p(b) \sim b^{\beta_1-1}(\lambda-b)^{\beta_2-1}$  supported on  $[0, \lambda]$ . Before addressing the issue of scale-correlations within a new context in Sect. 4, we quantify some  $\lambda$ -dependent properties of the unconditional breakdown coefficients.

Fig. 6 shows the second moment  $\langle b^2(\lambda, \Delta) \rangle$  of the breakdown coefficients as a function of  $\lambda$  and  $\Delta$ . They have been calculated for a typical length scale within the observed scale-independent regime  $20\eta \leq l \leq L$ . If the breakdown coefficients were identical to the random multiplicative weights  $q(l; \lambda)$  of Eq. (4), then the modified form

$$\tilde{\tau}_2(\lambda, \Delta) = \ln \langle b^2(\lambda, \Delta) \rangle / \ln \lambda \quad (8)$$

should reproduce the multifractal exponent  $\tau_2$ , which has served as input into the modeling (1). Evidently this is not the case. The apparent exponent  $\tilde{\tau}_2$  strongly depends on  $\Delta$  and  $\lambda$ . In Ref. [8] the empirical expression

$$\tilde{\tau}_2(\lambda, \Delta) = \tilde{\tau}_2(\Delta) + a(\Delta) \ln \ln \lambda \quad (9)$$

has been found to describe the experimentally observed  $\lambda$ -dependence with reasonable precision. As can be seen in Fig. 6, this expression also fits well to our simulational findings. Fitted parameters are  $\tilde{\tau}_2(\Delta = 0) = 0.14$ ,  $a(\Delta = 0) = 0.034$ , and  $\tilde{\tau}_2(\Delta = \pm 1/2) = 0.196$ ,  $a(\Delta = \pm 1/2) = 0.044$ . Neither for  $\Delta = 0$  nor for  $\Delta = \pm 1/2$  the corrected exponent  $\tilde{\tau}_2(\Delta)$  is able to reproduce the true  $\tau_2 = 0.24$ .

These findings show two things: first, the experimentally observed moment systematics (9) of breakdown coefficients is again fully reproduced by the stochastic process

(1), and, second, there is no need to argue which combination  $\lambda$ ,  $\Delta$  is best for the moments of breakdown coefficients to reproduce the correct scaling exponents. As to the latter point, Ref. [21] has conjectured that the best combination is  $\lambda = 2$ ,  $\Delta = \pm 1/2$ . In fact, another quick look at Fig. 6 reveals that this combination produces an apparent intermittency exponent which comes closest to the true one. Looking again at the construction (1)-(4) of our stochastic process, much better suited observables for the extraction of true multifractal exponents are the two-point correlation densities (5). See also Refs. [31,32] for related data analysis.

## 4 Apparent scale-correlations II: Kramers-Moyal coefficients

We discuss more apparent scale correlations obtained from the multifractal process (1)-(2). The moments

$$D_n(\ln \varepsilon_l; l, \lambda, \Delta) = \frac{1}{n! \ln \lambda} \langle (\ln b(l, \lambda, \Delta))^n | \ln \varepsilon_l \rangle \quad (10)$$

of logarithmic breakdown coefficients are conditioned on the logarithmic coarse-grained field. For  $\Delta = 0$  and a typical length scale, the  $1 < \lambda \leq 2$  dependence of the first two moments is shown in Fig. 7. A good empirical parametrization of the simulational results is given by

$$D_1(\ln \varepsilon_l; l, \lambda, \Delta) = a_{10}(l, \Delta) + a_{11}(l, \lambda, \Delta) (\ln \varepsilon_l - \langle \ln \varepsilon_l \rangle) + \dots \quad (11)$$

$$D_2(\ln \varepsilon_l; l, \lambda, \Delta) = a_{20}(l, \lambda, \Delta) + a_{21}(l, \lambda, \Delta) (\ln \varepsilon_l - \langle \ln \varepsilon_l \rangle) + \dots \quad (12)$$

All linear  $D_1$  curves are found to intersect at  $\ln \varepsilon_l = \langle \ln \varepsilon_l \rangle$ , which makes the coefficient  $a_{10}$  independent of  $\lambda$ . Already for  $\lambda = 2$  the slope  $a_{11}$  is positive and increases further, the smaller  $\lambda$  becomes. This positive correlation between logarithmic breakdown coefficient and logarithmic coarse-grained field appears to converge for  $\lambda$  sufficiently close to one. See also Fig. 8a, which illustrates the  $l$  dependence of  $a_{11}$  for various  $\lambda$ . As for the second-order moment, the slope coefficient  $a_{21}$  remains close to zero, being positive (negative) above (below)  $\lambda \approx 1.15$ . This makes  $D_2$  more or less independent of  $\ln \varepsilon_l$ , but not of  $\lambda$ . The coefficient  $a_{20}$  declines rapidly as  $\lambda$  becomes smaller; see also Fig. 8b.

For comparison, we give the respective unconditional moments of the log-normal random multiplicative weights of Eq. (4):

$$\langle \ln q \rangle / \ln \lambda = -\tau_2/2, \quad (13)$$

$$\langle \ln^2 q \rangle / 2 \ln \lambda = \tau_2/2 + (\tau_2^2/8) \ln \lambda. \quad (14)$$

These relations follow straightforwardly from the multifractal sum rules [32], which relate the cumulants of the logarithmic random multiplicative weights to the multifractal exponents. Except for a negligible  $2 \geq \lambda > 1$  dependence of (14), the two moments are constant. The difference between (13)-(14) and (11)-(12) demonstrates again

that the breakdown coefficients should not be mixed up with the random multiplicative weights.

However, the comparison of (11) with (13) leaves us with a surprising detail. Fig. 9 illustrates the  $l$  dependence of the coefficient  $a_{10}$ . The results for  $\Delta = 0$  and  $\Delta = \pm 1/2$  are almost identical and show only a very weak  $\ln l$  dependence. More or less the coefficient is constant and takes on the value  $a_{10} \approx -0.12$ , which coincides with (13). Without having a deeper explanation at hand, it appears that  $a_{10}$  allows to extract the value of the intermittency exponent with reasonable precision. – Due to (14), a similar extraction might also be successful from (12). A glimpse at Fig. 8b destroys this hope. The coefficient  $a_{20}$  strongly depends on  $\lambda$  and weakly on  $l$ . To some degree it also depends on  $\Delta$ . Except for  $\lambda = 2$ , its value is always well below  $\tau_2/2 = 0.12$  of (14).

If the moments (10) converge in the limit  $\lambda \rightarrow 1$ , they would become the Kramers-Moyal coefficients of the Markovian description of the turbulent energy cascade [9,10]. Since any data-driven extraction faces difficulties with this limit, two different operational definitions have been put forward: Ref. [9] uses a relative,  $l$  independent truncation at  $\lambda_1 = 1.04$ , whereas Ref. [10] employs an absolute, but  $l$  dependent truncation at  $\lambda_2 = l/(l - 4.4\eta)$ . We have adopted these two operational definitions with the small modifications  $\lambda_1 = 16/15$  and  $\lambda_2 = l/(l - 4\eta)$ , adopted to our numerical resolution of the multifractal process (1)-(2). Fig. 10 illustrates the model-based outcome for the drift coefficient  $\gamma(l) = a_{11}(l, \lambda, \Delta = 0)$  and the diffusion coefficient  $D(l) = a_{20}(l, \lambda, \Delta = 0)$ . The curves corresponding to the  $\lambda_1$  limit are identical to the  $\lambda = 16/15$  curves of Fig. 8; see also Fig. 7, where the two bold curves correspond to the two different limits. In the  $\lambda_1$  limit, the diffusion coefficient is more or less constant, whereas the drift coefficient increases to some extent with increasing length scale. Although the model has not been fitted to the low-temperature helium-jet data used in Ref. [9], the order of magnitude of the found drift and diffusion coefficient matches well the values  $\gamma = 0.21$  and  $D = 0.03$  stated in this reference. The  $\lambda_2$  limit results in an  $l$  dependence for the drift as well as the diffusion coefficient, which can be parametrized with  $\gamma(l) = 0.012(l/\eta)^{0.51}$  and  $D(l) = 0.32(l/\eta)^{-0.62}$ . Also shown in Fig. 10 are the expressions  $\gamma(l) = 0.32 - 0.05 \ln(L/l)$  and  $D(l) = 0.01(L/l)^{0.4}$  of Ref. [10], which again have been extracted from low-temperature helium-jet data. Whereas the functional forms are identical for the diffusion coefficient, the functional forms for the drift coefficient are a little different. However, orders of magnitude and trends are close by. – Overall, the model findings for both operational definitions of the  $\lambda \rightarrow 1$  limit are in good qualitative agreement with the experimental results stated in Refs. [9,10]. This shows that there is no need to argue whether the one definition is more sensitive than the other [10]. Even more important, this demonstrates that the observed scale correlations ( $\gamma \neq 0$ ) and scale-dependence ( $\gamma = \gamma(l)$ ,  $D = D(l)$ ) can not be interpreted as signatures for the turbulent energy cascade to deviate from a scale-independent and scale-uncorrelated multifractal process.

## 5 Conclusion

We have demonstrated that a homogeneous random log-normal multifractal process, which has no built-in scale correlations, is able to produce apparent scale correlations expressed by conditional distributions and moments of breakdown coefficients. Given the quantitative agreement reached between the model findings and the results extracted from turbulent data, we are now even tempted to claim that these apparent scale-correlations go hand in hand with non-conservative random multifractal processes. The former are a consequence of the latter and have to be there! In this respect, it would be interesting to check on scale correlations in other known multifractal processes, like for example Internet traffic engineering [33] and econophysics [34,35].

As to the energy cascade of fully developed small-scale turbulence, our findings demonstrate that random multifractal processes appear to contain more truth than previously anticipated. In this context it will be interesting to extend our discussions beyond synthetic energy dissipation fields. Synthetic turbulent velocity fields are well modelled by multiaffine processes [36–41] with no built-in scale correlations. Such processes might as well describe velocity-based scale correlations of the form reported in Ref. [42].

## References

1. A. Kolmogorov, Dokl. Akad. Nauk. SSSR **30**, 301 (1941)
2. D. Schertzer, S. Lovejoy, in *Turbulent Shear Flow 4*, edited by L.B. et.al. (Springer, Berlin, 1985), p. 7
3. C. Meneveau, K. Sreenivasan, Phys. Rev. Lett. **59**, 1424 (1987)
4. C. Meneveau, K. Sreenivasan, J. Fluid Mech. **224**, 429 (1991)
5. U. Frisch, *Turbulence* (Cambridge University Press, Cambridge, 1995)
6. K.R. Sreenivasan, R.A. Antonia, Annu. Rev. Fluid Mech **29**, 435 (1997)
7. K.R. Sreenivasan, G. Stolovitzky, J. Stat. Phys. **78**, 311 (1995)
8. G. Pedrizzetti, E. Novikov, A. Praskovsky, Phys. Rev. E **53**, 475 (1996)
9. A. Naert, R. Friedrich, J. Peinke, Phys. Rev. E **56**, 6719 (1997)
10. P. Marcq, A. Naert, Physica D **124**, 368 (1998)
11. B. Jouault, P. Lipa, M. Greiner, Phys. Rev. E **59**, 2451 (1999)
12. B. Jouault, M. Greiner, P. Lipa, Physica D **136**, 125 (2000)
13. B. Jouault, M. Greiner, Fractals **10**, 321 (2002)
14. J. Cleve, M. Greiner, Phys. Lett. A **273**, 104 (2000)
15. F. Schmitt, D. Marsan, Eur. Phys. J. B **20**, 3 (2001)
16. F. Schmitt, Eur. Phys. J. B **34**, 85 (2003)
17. J. Muzy, E. Bacry, Phys. Rev. E **66**, 056121 (2002)
18. P. Chainais, R. Riedi, P. Abry, IEEE Trans. Inf. Theory **51**, 1063 (2005)
19. P. Chainais, R. Riedi, P. Abry, Traitement du Signal **22**(1) (2005)
20. J. Schmiegel, J. Cleve, H. Eggers, B. Pearson, M. Greiner, Phys. Lett. A **320**, 247 (2004)
21. M. Nelkin, G. Stolovitzky, Phys. Rev. E **54**, 5100 (1996)
22. G. Samorodnitsky, M. Taqqu, *Stable non-Gaussian random processes* (Chapman & Hall, New York, 1994)
23. C. van Atta, T. Yeh, J. Fluid Mech. **71**, 417 (1975)
24. A. Chhabra, K. Sreenivasan, Phys. Rev. Lett. **68**, 2762 (1992)
25. E. Novikov, Appl. Math. Mech. **35**, 321 (1971)
26. E. Novikov, Phys. Fluids A **2**, 814 (1990)
27. M. Ossiander, E. Waymire, Ann. Statist. **28**, 1533 (2000)
28. S. Kida, J. Phys. Soc. Japan **60**, 5 (1991)
29. F. Schmitt, D. Lavallée, D. Schertzer, S. Lovejoy, Phys. Rev. Lett. **68**, 305 (1992)
30. D. Schertzer, S. Lovejoy, Physica A **185**, 187 (1992)
31. J. Cleve, M. Greiner, B. Pearson, K. Sreenivasan, Phys. Rev. E **69**, 066316 (2004)
32. J. Cleve, T. Dziekan, J. Schmiegel, O. Barndorff-Nielsen, B. Pearson, K. Sreenivasan, M. Greiner, Phys. Rev. E **71**, 026309 (2005)
33. R.H. Riedi, M.S. Crouse, V.J. Ribeiro, R.G. Baraniuk, IEEE Transactions on Information Theory **45**(4), 992 (1999)
34. J. Muzy, J. Delour, E. Bacry, Eur. Phys. J. B **17**, 537 (2000)
35. E. Bacry, J. Delour, J. Muzy, Phys. Rev. E **64**, 026103 (2001)
36. R. Benzi, S. Ciliberto, R. Tripiccion, C. Baudet, F. Masaioloi, S. Succi, Phys. Rev. E **48**, 29 (1993)
37. A. Juneja, D. Lathrop, K.R. Sreenivasan, G. Stolovitzky, Phys. Rev. E **49**(6), 5179 (1994)

38. F. Elliott, A. Majda, D. Hornthrop, R. McLaughlin, *J. Stat. Phys.* **81**, 717 (1995)
39. A. Arneodo, E. Bacry, J. Muzy, *J. Math. Phys.* **39**, 4142 (1998)
40. S. Basu, E. Foufoula-Georgiou, F. Porte-Agel, *Phys. Rev. E* **70**, 026310 (2004)
41. O. Barndorff-Nielsen, J. Schmiegel, Research Report 4, Thiele Centre, Univeristy of Aarhus (2005)
42. C. Renner, J. Peinke, R. Friedrich, *J. Fluid Mech.* **433**, 383 (2001)

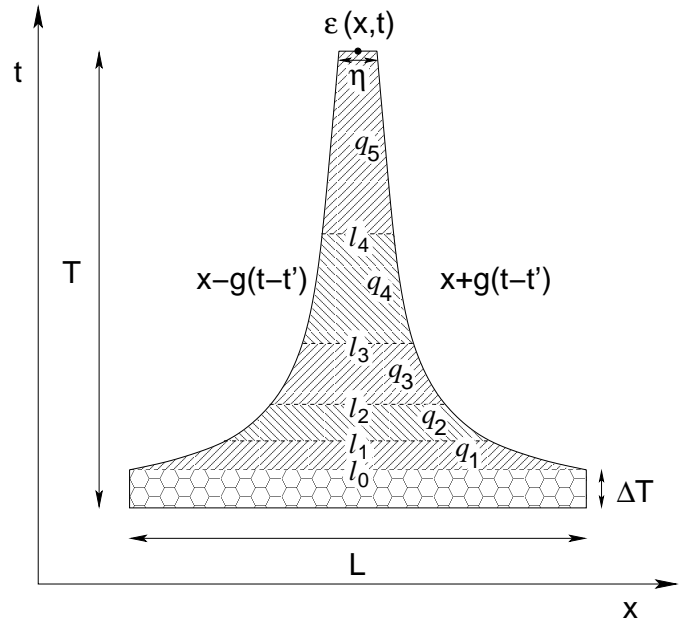


**Fig. 1.** Causality cone  $g(t-t')$  defined by Eq. (2), which enters into the construction (1) of the multifractal field  $\varepsilon(x, t)$ . The length and time scales  $\eta \ll L$  and  $\Delta T \ll T$  determine the multifractal scaling range. Also marked is the hierarchy of length scales  $l_j = L/\lambda^j$  confined by  $\eta = l_J$  and  $L = l_0$ ; for illustration  $J = 5$  has been chosen. The hatched stripes represent the associated random weights  $q_j$  of Eq. (4). Since the stripes are of equal size and do not overlap, the random weights are iid and not correlated. This leaves the multifractal process (1) without scale correlations. The honeycombed stripe with length  $L$  and width  $\Delta T = (\eta/L)T$  at the bottom of the causality cone is independent from, but not iid to the random multiplicative weights  $q_j$ ; it is introduced to produce perfect multifractal scaling of the two-point correlation densities (5).

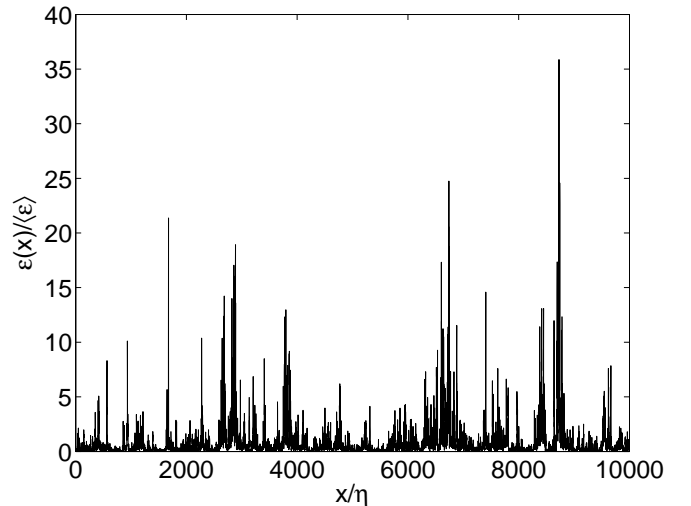


**Fig. 2.** Simulated equal-time trace of the multifractal field (1). Parameters are  $L/\eta = 500$ ,  $\alpha = 2$  and  $\tau_2 = 0.24$ . Only a representative fraction of the trace is shown.

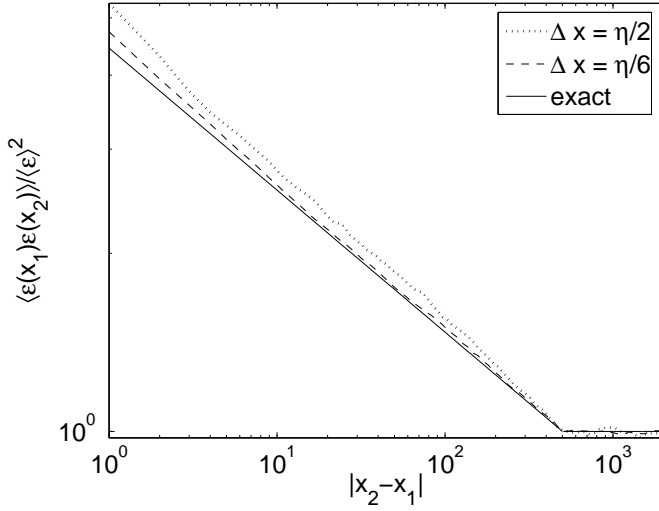


**Fig. 3.** Dependence of the sampled lowest-order equal-time two-point correlation density on the numerical resolutions employed for the simulated multifractal field (1). The numerical resolutions are  $\Delta x = \Delta t = \eta/6$  (dashed curve),  $\eta/2$  (dotted curve) for the Lévy-stable white-noise field  $\gamma(x, t)$  and  $\Delta x = \eta$  (dashed as well as dotted curve) for the equal-time trace  $\varepsilon(x)$ . For comparison the exact theoretical result (5) is also shown (solid curve). Used model parameters are  $L/\eta = 500$ ,  $\alpha = 2$  and  $\tau_2 = 0.24$ .

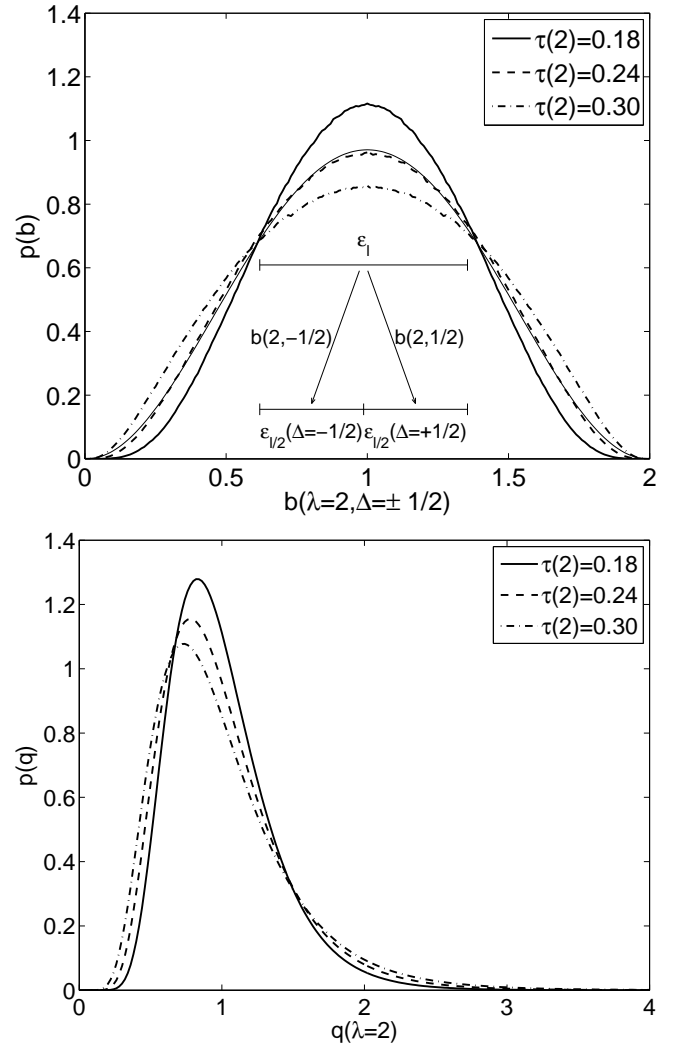


**Fig. 4.** (a) Unconditional distributions of breakdown coefficients  $b(\lambda, \Delta)$  with  $\lambda = 2$ ,  $\Delta = \pm 1/2$  (see inset) at scale  $l = 32\eta$  within the scale-independent regime  $20\eta < l < L$ . They have been sampled from model traces with parameter settings  $\alpha = 2.0$  and  $\tau(2) = 0.18$  (solid),  $0.24$  (dashed),  $0.30$  (dash-dotted). For comparison a symmetric Beta distribution  $p(b) \sim b^{\beta-1}(2-b)^{\beta-1}$  with  $\beta = 3.2$  is also shown (thin solid), which has been reported in the analysis of a high-Reynolds number turbulent flow [7]. (b) For comparison, respective log-normal distributions  $p(q)$  for the random  $\lambda=2$  multiplicative weights of Eq. (4) are also shown. They are not identical to the distributions of breakdown coefficients.

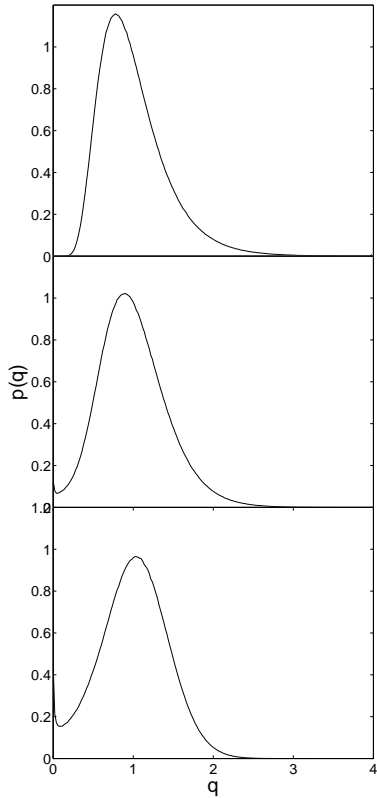
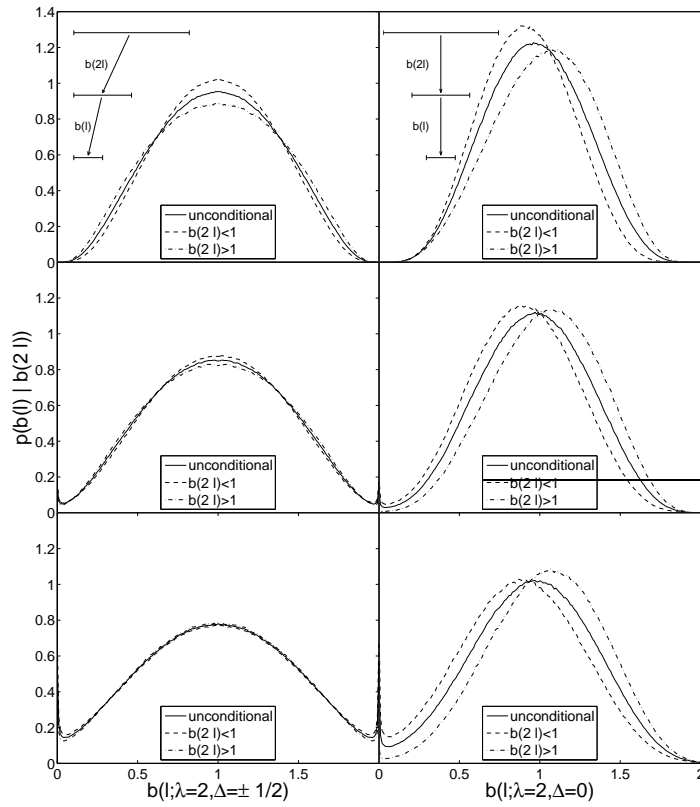


**Fig. 5.** (a) Unconditional and conditional distributions of breakdown coefficients for  $\lambda = 2$ ,  $\Delta = \pm 1/2$  (first column), 0 (second column), at the typical scale  $l = 32\eta$ . From top to bottom row the stable index has been set to  $\alpha = 2, 1.7, 1.4$ . The intermittency exponent has been fixed to  $\tau_2 = 0.24$ . (b) For comparison, respective log-stable distributions  $p(q)$  for the random  $\lambda = 2$  multiplicative weights of Eq. (4) are shown in the third column.

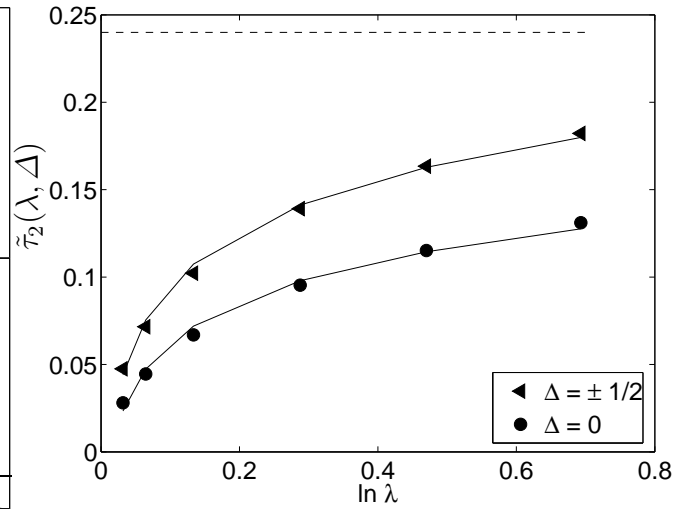


**Fig. 6.** Apparent intermittency exponent  $\tilde{\tau}_2 = \ln \langle b^2(\lambda, \Delta) \rangle / \ln \lambda$  as a function of the scale ratio  $\lambda$  for  $\Delta = \pm 0.5$  (triangle) and 0.0 (bullet). The second moment of the breakdown coefficients has been calculated for a typical length scale within the scale-independent regime. The solid curves represent a fit according to the suggestion (9) of Ref. [8]. For comparison, the dashed line shows the true  $\tau_2 = 0.24$ , which together with  $\alpha = 2.0$  has served as model input.

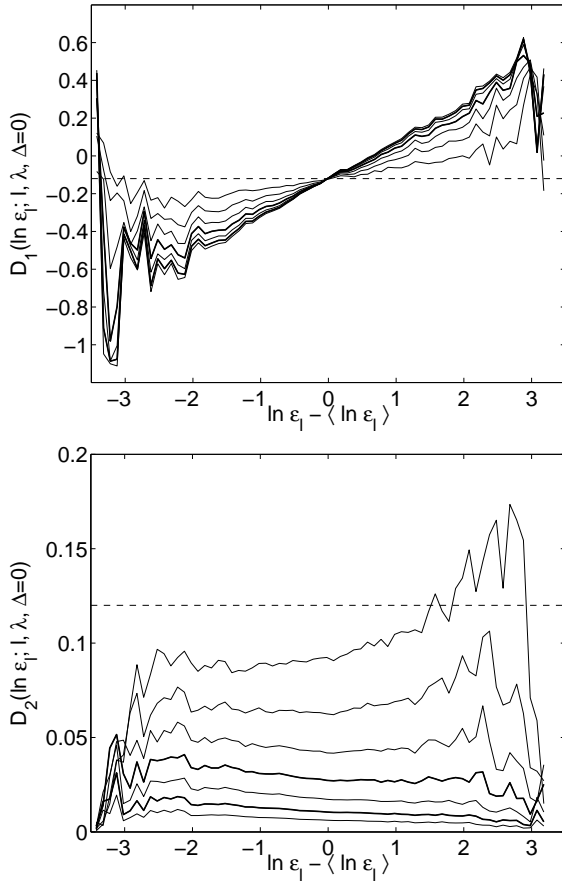


**Fig. 7.** Conditional first- (top) and second-order (bottom) moments  $D_n(\ln \varepsilon_l; l, \lambda, \Delta)$  of breakdown coefficients for  $\lambda = 2, 4/3, 8/7, 16/15$  (bold),  $32/31, 64/63$  (bold) and  $128/127$  (curves with increasing slope for  $D_1$ , and from top to bottom for  $D_2$ ). Parameters are  $\Delta = 0$  and, as a typical length scale,  $l = 256\eta$ . The moments have been sampled from simulated traces of the multifractal process (1)-(2) with parameter settings  $\alpha = 2.0$  and  $\tau_2 = 0.24$ . For comparison also the moments (13) and (14) (with  $\lambda = 1$ ) are shown as dashed lines.

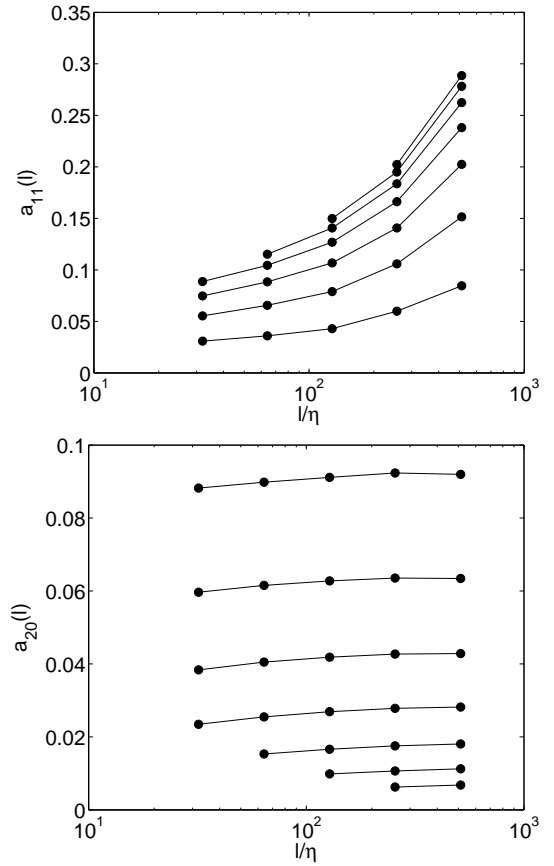


**Fig. 8.** Coefficients  $a_{11}$  (top) and  $a_{20}$  (bottom) of Eqs. (11) and (12) as a function of  $l$  for  $\lambda = 2, 4/3, 8/7, 16/15, 32/31, 64/63, 128/127$  ( $a_{11}$ : from bottom to top,  $a_{20}$ : from top to bottom) and  $\Delta = 0$ . They have been obtained from simulated traces of the multifractal process (1)-(2) with parameter settings  $\alpha = 2.0$  and  $\tau_2 = 0.24$ .

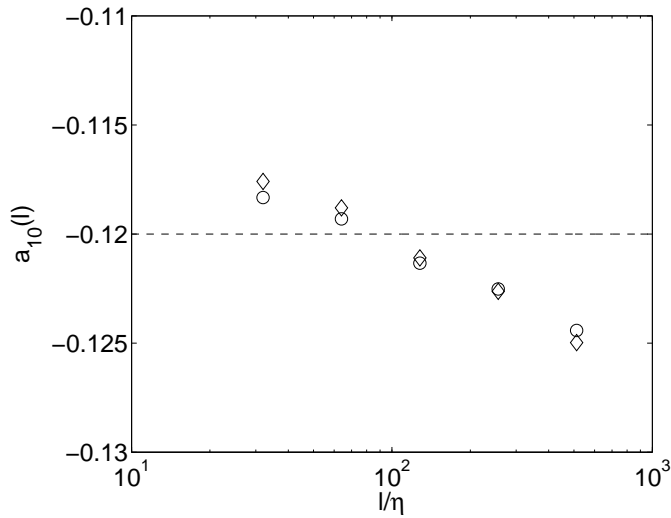


**Fig. 9.** The  $\lambda$  independent coefficient  $a_{10}$  of (11) as a function of the length scale  $l$  for  $\Delta = 0$  (circles) and  $1/2$  (diamonds). It has been obtained from simulated traces of the multifractal process (1)-(2) with parameter settings  $\alpha = 2.0$  and  $\tau_2 = 0.24$ . For comparison the constant (13) is shown as the dashed line.

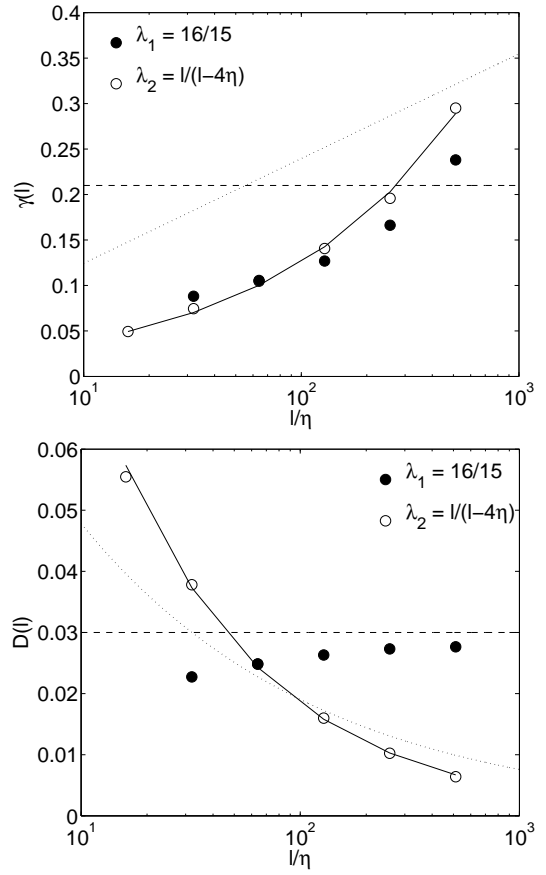


**Fig. 10.** (a) Drift coefficient  $\gamma(l) = a_{11}(l, \lambda, \Delta = 0)$  and (b) diffusion coefficient  $D(l) = a_{20}(l, \lambda, \Delta = 0)$  as a function of the length scale  $16\eta \leq l \leq L$ . The two operational definitions  $\lambda_1 = 16/15$  and  $\lambda_2 = l/(l - 4\eta)$  are shown with full and open circles, respectively. For the latter, the solid curves represent the parameterizations  $\gamma(l) = 0.012(l/\eta)^{0.51}$  and  $D(l) = 0.32(l/\eta)^{-0.62}$ . The coefficients have been obtained from simulated traces of the multifractal process (1)-(2) with parameter settings  $\alpha = 2.0$  and  $\tau_2 = 0.24$ . For comparison, the  $\lambda_1$  result (dashed) of Ref. [9] and the  $\lambda_2$  result (dotted) of [10] are shown, which have been extracted from a low-temperature helium-jet flow.